J Mater Sci: Mater Electron (2017) 28:721–728
DOI 10.1007/s10854-016-5582-2

The fabrication of Al–diamond composites for heat dissipation by liquid–solid separation technology

Hongyu Zhou[1] · Yanli Yin[2] · Zhongliang Shi[3] · Chunjing Wu[1] · Junyou Liu[1,2]

Received: 7 June 2016 / Accepted: 17 August 2016 / Published online: 24 August 2016

Abstract Low-cost and good quality Al–diamond composites were prepared in the application of heat dissipation using an advanced liquid–solid separation technology. Their thermal conductivity (TC) and coefficient of thermal expansion (CTE) were measured, especially on the effect of diamond particle surface metallization. The TC of composites reinforced with Ni-coated diamond particles was found to have increased by almost 80 % compared to that of Al alloys. The diamond surface in the composites was characterized using an electron microprobe, X-ray diffraction and SEM. It was found that high TC of the composites was obtained due to the generation of Al_4Ni_3 and AlNi phases at their interfaces between Al and diamond. In addition, the theoretical calculation for TC and CTE of the composites show the similar tendency with their experimental data.

1 Introduction

The development of miniaturization and integration of electronic devices has led to the rapid increase of heat transfer rate within unit volume, suitable packing materials must have excellent thermal conductivity (TC) to dissipate heat effectively, in order to ensure high reliability of the electronic devices and modules [1–3]. Diamond particles are currently investigated on account of the highest TC (1200–2000 W m^{-1} K^{-1}), combined with a low coefficient of thermal expansion (CTE) that can effectively meet the demands of semiconductor-based devices [4–6]. Al-matrix composites reinforced with diamond particles can be designable with required high TC, suited CTE as well as low density [7, 8].

There are several methods for the manufacture of Al–diamond composites with very good thermo-physical property. Of course the methods are expected that can realize near-net-shape fabrication with a relatively inexpensive cost [9, 10] because the composite is quite difficult to machine. For example, Infiltration process (such as Pressureless Infiltration [11], Squeeze Pressure Infiltration [6] and Gas Pressure Infiltration [12]), Spark Plasma Sintering [13] and Vacuum Hot Pressing [14] have already been investigated, however these processes are not suitable for the requirement of the large scale manufacture. So we need to find a suitable process to build the composite easily with less machining. As we know, the thermal properties of Al–diamond composites are subjected to the detail processing conditions of fabrication [15], especially determined by the wettability between Al-alloy matrix and the ceramic reinforcement [16]. So there are usually three methods to enhance the wetting of the interface [17]: (1) to modify the diamond surface based on the chemical process; (2) to coat an active metal layer on the diamond surface; (3) to form a layer of metallic carbide on the diamond surface (such as Al_4C_3).

This study aims to propose an advanced liquid–solid separation (LSS) technique to fabricate Al-based composites reinforced by Ni-coated diamond and to investigate into how to improve their thermal properties through based on the changes of diamond particle surface coating. Meanwhile, The TC of the composites is also calculated

✉ Junyou Liu
ljy158@yeah.net

[1] School of Materials Science and Engineering, University of Science and Technology Beijing, Beijing, China

[2] Institute of Emerying Technology and Industry, University of Science and Technology Beijing, Beijing, China

[3] School of Materials Science and Engineering, Jiangsu University, Zhenjiang, China

using Maxwell and Differential Effective Medium (DEM) theoretical models and the CTE of the composites is also calculated by Kerner model as well.

2 Experimental procedures

2.1 Preparation of raw materials

Pure aluminum (99.81 wt%) having an average particle size about 37 μm being a matrix material, was purchased from Zhengzhou Aerospace Aluminum Co., Ltd. in China. Synthetic single crystal diamond particles of the HFD-B type were selected to be as reinforcement. HFD-B is manufacturer's product model of diamond which is equivalent to MBD-4 and its average sizes were about 106 μm. These diamond particles were manufactured by Henan Huanghe Whirlwind Co., Ltd. in China. Its nitrogen level was approximately 190–200 ppm and the inherent TC was about 1500 W m^{-1} K^{-1}. The intrinsic TC of diamond would be reduced if the concentration of nitrogen increased [18]. It was reported [19] that the element Ni in the matrix or at the diamond surface with a layer thinner than 1 μm could more effectively increase the interfacial thermal conductance (ITC) and TC of the composites. Diamond particles coated with the nickel nanoscale layer by vacuum ion plating were wrapped. The layer thickness was about 100 nm. The characteristics of raw materials and particle size distribution were presented in Table 1.

2.2 Preparation of the composites

Al–diamond composites used for electronic package materials were prepared by LSS technique [20, 21]. The schematic of the die for LSS process is shown in Fig. 1.

Figure 2 showed the melting temperature of pure aluminum measured using DSC linear extrapolation. It was found that the initial and end temperatures of melting were 658.7 and 682.7 °C respectively. So the heating temperature of the cold press blank was set around 683 °C in order to acquire semi-solid slurry. The SEM image taken from the liquid material squeezed out through the 2 mm filter during liquid–solid separation was shown in Fig. 3. It was not easy to find the single crystal diamond particles from the separated material in above liquid phase. This indicated that the 2 mm filter could efficiently interrupt diamond particles to effuse and permeate into the separated liquid. However, there might have also some air left between metal matrix and the reinforced phase during compressing molding [9], the filter tanks of the die used for LSS process could not only squeeze out the pure liquid aluminum, but also rapidly reduce the left air and realize the composites in high quality. Besides, LSS process could also prepare functionally gradient materials (FGMs) that we would recommend in our future study.

Table 1 Characteristics of raw materials and particle size distribution

Material	D (10) (μm)	D (50) (μm)	D (90) (μm)	Span
Aluminum	15.922	37.279	84.176	1.83
HFD-B	72.872	106.104	153.848	0.76
HFD-B-Ni	74.402	103.158	142.771	0.66

The detail process for the fabrication of the composites was described as following: aluminum with about 20 vol% diamond powders were mechanically mixed about 4 h, followed by cold-press forming at 500 MPa for 1 min, then with a heating rate of 30 °C min^{-1}, the material was remelted into semi-solid state at 683 °C for 40 min. After that, we used LSS process to separate the liquid aluminum and the solid diamond under the pressure of 50 MPa and held this pressure for 15 min. The quantitative liquid was separated from the composites through these 2 mm filter tanks and the retained part would be the composite reinforced with 40 vol% diamond. The fabricated composite for the application of heat dissipation was shown in Fig. 4. Its size was about 50 mm × 40 mm × 3 mm.

2.3 Characterization and properties measurements of the composites

Based on all measurement requirements, the Al–diamond composite samples were machined by laser cutting machine and diamond wheel grinder. The melting temperature of aluminum used was determined by SDTQ 600 simultaneous thermal analyzer (DSC, TA, America) with a heating rate of 10 °C min^{-1}. The surface microstructures of the diamond powders and three-point bending fracture of Al–diamond composites were observed by an EVO-18 scanning electron microscope (SEM, ZEISS, Germany). The line scanning distributions of main elements between aluminum matrix and reinforced phase were detected using a JXA-8230 electron microprobe analysis (EMPA, JEOL, Japan). The phase composition of the composites was confirmed by D-MAX-RB X-ray diffraction (XRD, RIGAKU, Japan), diffractometer using Cu target, operating voltage was 40 kV and working current was 150 mA. The density (ρ) of the alloys was measured by GH-120E automatic density measuring instrument (UNLONG, China). The thermal diffusion values (α) of the sample having size of ϕ 12.7 mm × 3 mm, was tested by a LFA 427 laser flash thermophysical machine (NETZSCH, Germany) at room temperature. The specific heat capacity (C_p) was based on the theoretical calculation. The TC (λ) can be obtained by formula: $\lambda = \rho \times \alpha \times C_p$. The CTE of the sample having size of 3 mm × 4 mm × 25 mm, was gauged by a DIL 402C differential dilatometer

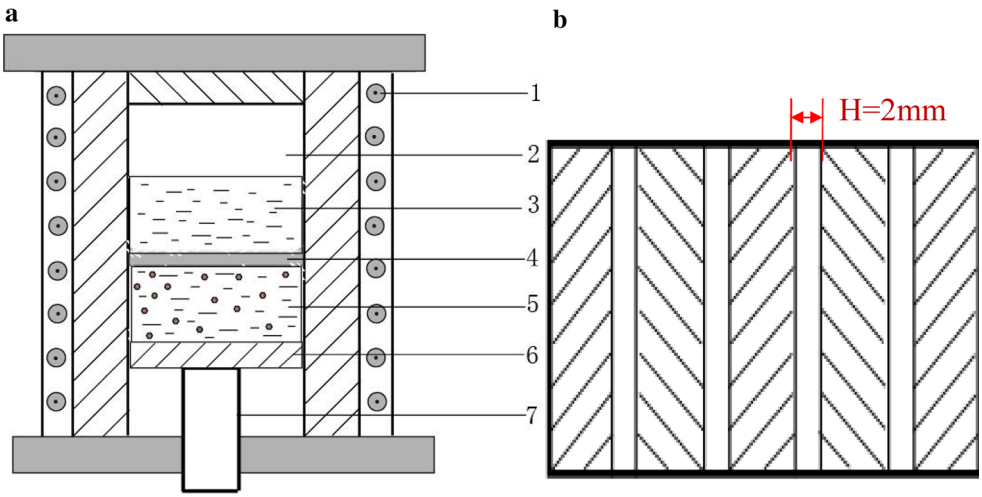

Fig. 1 Schematic diagram of the die of LSS (**a**): *1* resistance wire; *2* cavity of upper die Chamber; *3* liquid of separate out; *4* separation channel (**b**); *5* cold press blank; *6* down pattern plate; *7* ejector pin

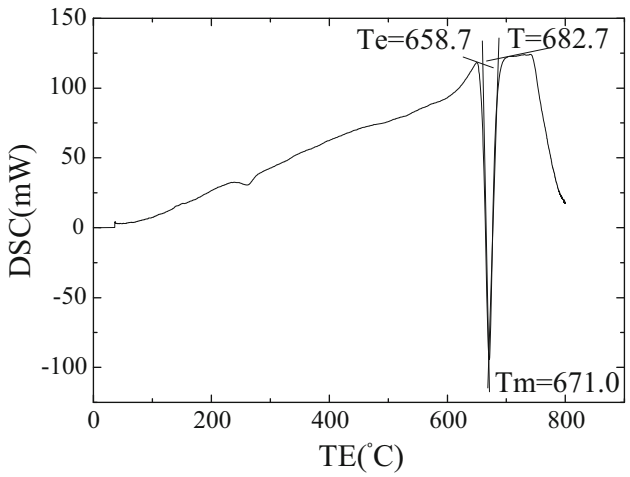

Fig. 2 Melting temperature of purity aluminum, detected by DSC

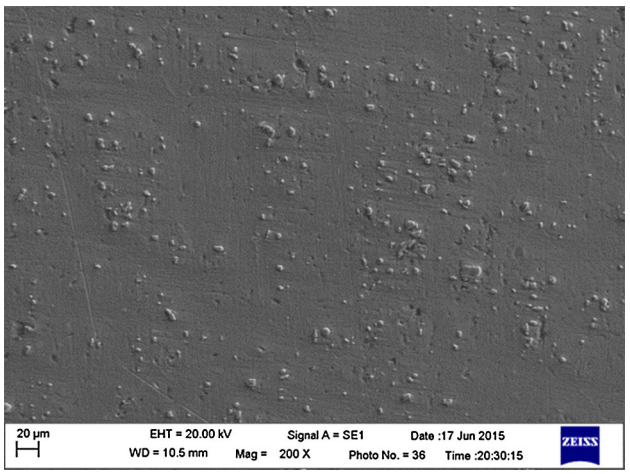

Fig. 3 Solidified microstructure observed from squeezed out the liquid phase

Fig. 4 The fabricated composite in the application of heat dissipation prepared by LSS process

(NETZSCH, Germany) and the temperature range was from room temperature to 200 °C at a heating rate of 5 °C min^{-1}. The gas tightness of the composites was detected by ZQJ-530 helium mass spectrometer leak detector (KYKY, China) at a pressure of 5 MPa for 4 h. The three-point bending (σ_f) test was carried out by a RGM-3010 electronic universal testing machine (REGER, China), and the sample dimensions was 3 mm × 4 mm × 25 mm.

3 Results and discussion

3.1 Surface topography of used raw materials

The SEM morphologies of diamond particles with or without Ni-plated were shown in Fig. 5. It can be seen that the surface of the single diamond having a uniform size

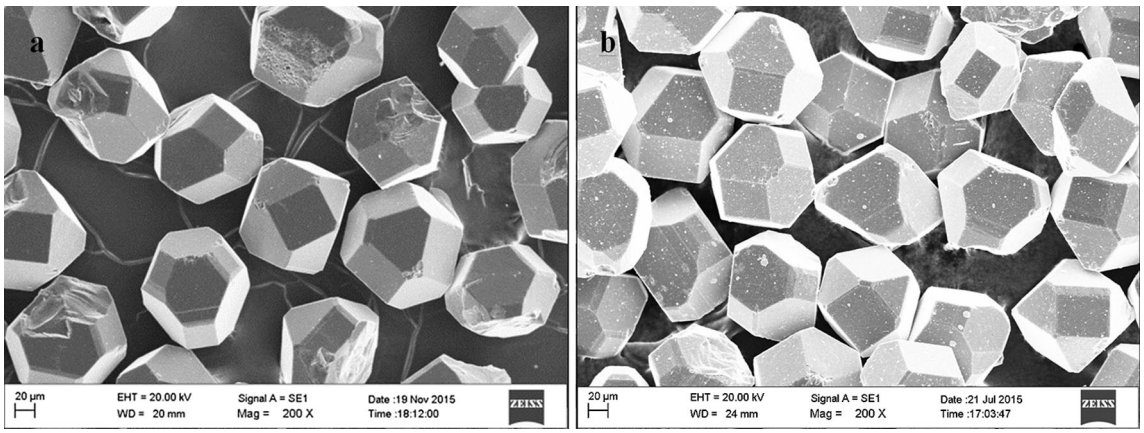

Fig. 5 SEM morphologies showing the diamond particles and their surfaces: HFD-B (**a**), HFD-B-Ni (**b**)

was smooth and regular, in Fig. 5a. Figure 5b obviously showed a homogeneous and consecutive coating layer at the surface of the diamond particles after coated with Ni.

3.2 Interfacial behavior

The interfaces of Al–diamond composites were analyzed using EMPA in order to understand the interfacial reaction and combination. The EMPA image and EDS spectra shown in Fig. 6 illustrated the liner distributions of elements C (blue curve), Al (pink curve) and Ni (green curve) of interfacial bonding areas. Based on the EDS spectra in Fig. 6b, there was only a small diffusion zone between Al and diamond because of low solid solubility between Al and diamond (C). However, the element Ni was clearly diffused into aluminum matrix from the coated layer at the surface of diamond powders.

In order to clearly understand the interfacial reaction between Ni-coated diamond and aluminum of the composites, the XRD patterns from the composite built by LSS process were shown in Fig. 7. Only were Al and diamond identified in the Al–diamond composites.

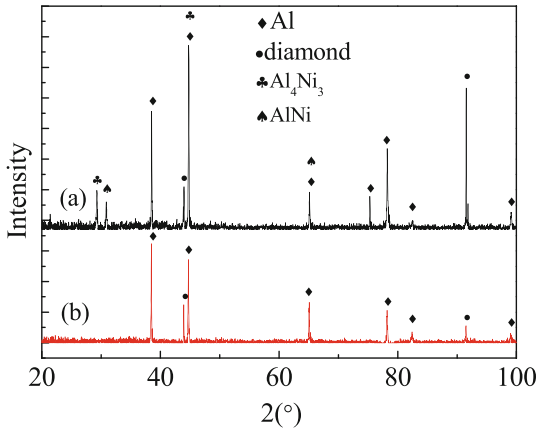

Fig. 7 XRD patterns of composites: Al–Ni–diamond (**a**), Al–diamond (**b**)

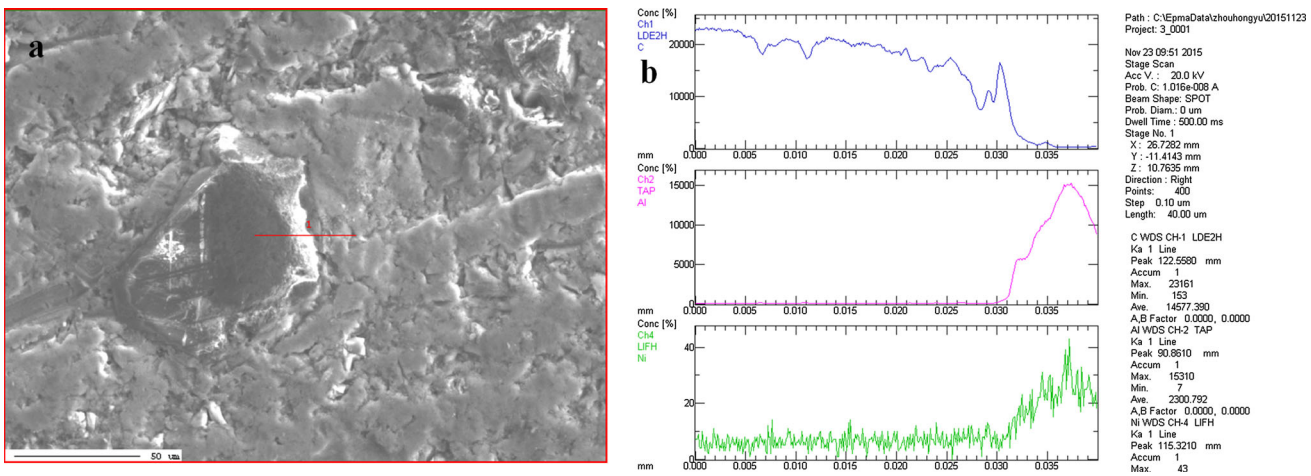

Fig. 6 EMPA image showing the measured position (**a**), corresponding EDS results (**b**)

However, the XRD patterns from the composite reinforced with Ni-coated diamond showed some additional peaks that were confirmed the presence of Al_4Ni_3 and AlNi phases. The interfacial reactions could play the key role between the Al matrix and the diamond. These Al–Ni intermetallics might be a bridge and well linked the Al matrix and the diamond. On the one hand, the combination of Ni coated on the diamond using vacuum ion plating was relatively strong. On the other hand, the formation of Al–Ni intermetallics was beneficial to build aluminum matrix stronger and kept away from the Al_4C_3 phase. It was noteworthy that there was no Al_4C_3 phase in the XRD patterns, as a result of the composite was fabricated at temperature of less than 800 °C [22].

3.3 Interface topography

Figure 8 showed the SEM images that were taken from the three-point bending fracture surfaces of two different composite samples fabricated by LSS process. The samples were reinforced by diamond and Ni-coated diamond powders. They were: (a) HFD-B and (b) HFD-B-Ni respectively. The observation for these fracture surfaces revealed that the diamond particles either uncoated or Ni-coated particles were well embedded into the Al matrix and no clear pores around the interfaces could be observed, which indicated that the composites fabricated by LSS process would have high densities and good properties in the application of heat dissipation. However, the fracture surfaces as shown by the red arrows in Fig. 8a were very clean and exposed the bare diamond surfaces which demonstrated the weak interfacial bonding between Al matrix and these uncoated diamond particles. Figure 8b showed the fracture surfaces of the composite reinforced with Ni-coated diamond particles. It could be seen that diamond particles were partially covered by aluminum matrix and these fractures were not fully open structure. This phenomenon indicated that the interfacial bonding between aluminum matrix and Ni-coated diamond particles was greatly enhanced, which was consistent with the above XRD analysis.

3.4 Mechanical properties

The effect of diamond particle surface metallization on the relative density of the composites was listed in Table 2. The composites reinforced with Ni-coated diamond particles had the best densification than these uncoated ones. This consequence indicated that high relative density was dependent on the interfacial wetting between Al and diamond particles. Ni-coated layer played a role in the combination like a bridge between Al and diamond. Moreover, studies had corroborated that the relative density of composites was crucial to thermal properties [1, 9].

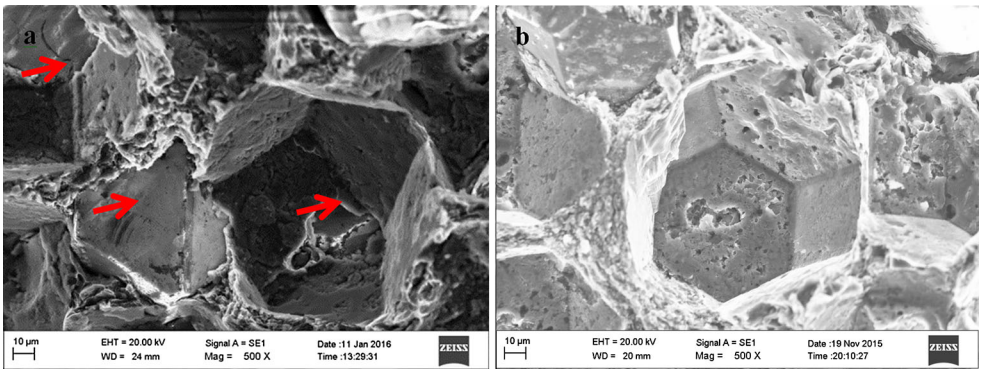

Fig. 8 SEM morphologies showing the fracture surfaces reinforced with: Al-B (**a**), Al-B-Ni (**b**)

Table 2 Physical properties of Al and Al–diamond composites

Sample	ρ (g cm^{-3}) (relative density, %)	C_p (J g^{-1} k^{-1})	α (mm^2 s^{-1})	TC (W m^{-1} K^{-1})	CTE (10^{-6} K^{-1})	σ_f (Mpa)	Gastightness (10^{-9} Pa m^3 s^{-1})	Source
Bulk Al	2.698	0.895	–	237	23.5	–	–	[23, 24]
Diamond	3.500	0.5	–	1200–2000	1.2	230–480	–	[4–6, 25]
Al-B	2.933 (97.22)	0.742	70.37	153.10	12.3	106.08	4.8	
Al-B-Ni	2.960 (98.05)		77.52	173.47	12.6	112.43	5.0	
Pure Al	2.657 (98.59)	0.895	41.3	98.21	24.3	222	3.6	

It was clear to see the mechanical and physical properties of Al and Al–diamond composites in Table 2:

(a) Relative density was the decisive factor for the properties of TC and σ_f, but it had less effect on CTE of the composite, respectively.
(b) Except CTE values, the composite reinforced with Ni-coated diamond particles exhibited better properties than that composites reinforced with uncoated diamond particles.
(c) The TC values in the Al–diamond composites were better than that of pure Al, but lower than that of bulk Al.

3.5 Thermal conductivities

In order to clearly understand which TC of Al–diamond composites are related to, we will describe its theoretical predictions as following, combined with above analysis of the experimental results.

These factors for the TC of Al–diamond composites, such as geometric characteristics and volume fractions of reinforcements, as well as phase properties [7, 15, 19] are given. Among other theoretical predictions for TC of the composites (λ_C), the scheme of Maxwell [26] and DEM [27, 28] were more systematically, which can be indicated respectively as:

$$\text{Maxwell}: \lambda_C = \frac{\lambda_m \times \left[2 \times \lambda_m + \lambda_d^{eff} + 2 \times \left(\lambda_d^{eff} - \lambda_m\right) \times V_d\right]}{2 \times \lambda_m + \lambda_d^{eff} - \left(\lambda_d^{eff} - \lambda_m\right) \times V_d} \quad (1)$$

$$\text{DEM}: \left(\frac{\lambda_C}{\lambda_m}\right)^{\frac{1}{3}} (1 - V_d) = \frac{\frac{\lambda_d^{eff}}{\lambda_m} - \frac{\lambda_C}{\lambda_m}}{\frac{\lambda_d^{eff}}{\lambda_m} - 1} \quad (2)$$

where λ_m is the TC of the matrix (in this case pure Al, $\lambda_m = 98.21$ W m^{-1} K^{-1}), V_d is the reinforcement volume fraction, λ_d^{eff} is the effective TC of the reinforcement particles according to equation:

$$\lambda_d^{eff} = \frac{\lambda_d^{in}}{1 + \frac{\lambda_d^{in}}{r \times h_C}} \quad (3)$$

where r was the radius of reinforcement; λ_d^{in} was the TC of the diamond (1500 W m^{-1} K^{-1}), was the interface thermal conductance (ITC), which can be back-calculated by using the acoustic mismatch model, like Eq. (4). The calculations between aluminum and diamond are listed in Table 3. C_p was the specific heat of the matrix, ρ as the density of the matrix, η_{1-2} was the transmission coefficient of phonons across from matrix to reinforcement and C_D was the Debye velocity of the matrix:

$$h_C = \frac{1}{4} \times \rho \times C_p \times \eta_{1-2} \times C_D \quad (4)$$

in the calculations, the Debye velocity can be theoretically established, expressed as follows:

$$C_D = \frac{1}{\sqrt{\frac{1}{2} \times \left(\frac{1}{c_l^2} \times \frac{1}{c_t^2}\right)}} \quad (5)$$

where c_l and c_t were the longitudinal and transversal phonon velocities across the matrix, respectively. The transmission coefficient for the acoustic mismatch model was defined as:

$$\eta_{1-2} = \frac{2 \times Z_1 \times Z_2}{(Z_1 \times Z_2)^2} \times \left(\frac{c_1}{c_2}\right)^2 \quad (6)$$

where the Z_i and c_i were the acoustic impedance ($Z = \rho \times c$) and the sound velocity for each phase with $i = 1, 2$.

The TC of the Al–diamond composites fabricated by LSS process was measured as shown in Fig. 9. As seen in the figure, the variation trend of TC was consistent with that of relative density. The performance of the composites was greatly improved, after the diamond particles were coated with nickel. The best value of TC in the composite

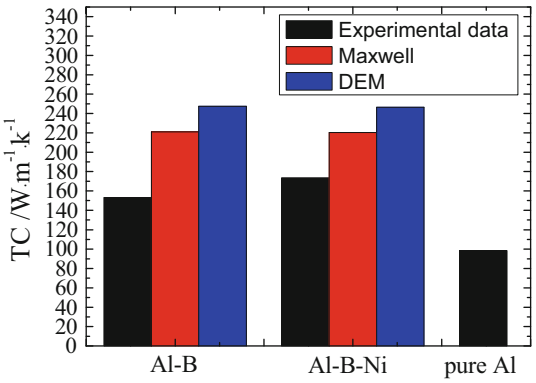

Fig. 9 Experimental data and theoretical predictions for the TC in Al–diamond composites reinforced with different diamonds

Table 3 Thermo-physical parameter of the different materials [29–31]

Sample	c_l (m s^{-1})	c_t (m s^{-1})	c_D (m s^{-1})	η_{1-2}	h_C (W m^{-2} K^{-1})	K (GPa)	G (GPa)
Aluminum	6240	3400	3865	0.019	4.43×10^7	66.3	25.4
Diamond	2000	12,300	14,817			440	550

reinforced with Ni coated diamond particles was 173.5 W m^{-1} K^{-1}, which were approximately 78.5 % (Maxwell) and 70.1 % (DEM), and it was 11.7 % over than that of the composite reinforced with the uncoated diamond.

The value of TC for the composite reinforced with Ni-plated diamond was close to the theoretical calculation, which could explain that the interfacial reaction could generate a useful thermal reaction layers and improve the interfacial wet-ability which was crucial to decrease the acoustic mismatch between Al matrix and diamond reinforcement [19]. It was remarkable that the porosity in the composites was not considered in the theoretical predictions, because the porosity could also enhance the phonon scattering and reduce the value of TC in the composites [32]. However, the measured value was actually lower than the ideal one. Based on the measured values of TC in the composites, we found that Ni-coated diamonds used as reinforcement could improve the TC value in the composite.

In comparison, pure Al was fabricated using the same process (LSS), as indicated in Table 2. The value of TC, only 98 W m^{-1} K^{-1}, was much different from the reference value of 237 W m^{-1} K^{-1}. The key reason might form a dense layer of alumina on the surface of aluminum particles that was about 35–40 W m^{-1} K^{-1} [9]. Meanwhile, the Al based composites reinforced with diamonds might be also the same reason to obtain low TC.

3.6 Coefficients of thermal expansion

The scheme of Kerner [33] has been applied widely to calculate the theoretical CTE model of the composites, because the model takes into account not only the microstress of the composites, but also the shear effect of grain boundary. The Kerner takes the following equation:

$$\alpha_c = \alpha_m V_m + \alpha_d V_d + V_d V_m(\alpha_d - \alpha_m) \times \frac{K_d - K_m}{V_m K_m + V_d K_d + \frac{3K_d K_m}{4G_m}} \quad (7)$$

where α_c is the CTE of the composites, α_m and α_d are the CTE of the matrix and the reinforcement respectively, V_m and V_d are the volume fraction of the matrix and the reinforcement in the composites respectively, K_m and K_d are the bulk modulus of the matrix and the reinforcement respectively, G_m is the shear modulus of the matrix.

A comparison of experimental data and the theoretically prediction of CTE for Al based composites reinforced with uncoated or Ni-coated diamonds were shown in Fig. 10. The measured CTE of the composites were about 12.3×10^{-6} K^{-1} and 12.6×10^{-6} K^{-1} respectively, which were lower than the theoretical value of Kerner (12.7×10^{-6} K^{-1}) and much less than the value of pure Al

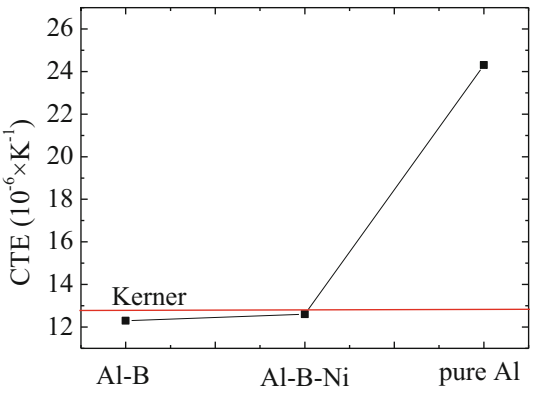

Fig. 10 Experimental data and theoretical predictions of CTE for Al-based composites reinforced with diamonds in different conditions

(24.3×10^{-6} K^{-1}). This indicated that the diamonds could afford a relatively large contribution to the CTE of composites, no matter what conditions of the diamonds and densification of the composites were.

3.7 Hermetic package

The air tightness of the composites was obtained under the condition of high pressure helium gas adsorption test. As a result, the air leakage rate of the composites kept stable within the range of $3.6–5.0 \times 10^{-9}$ Pa m^3 s^{-1}, which satisfied completely the requirements of the electronic packaging (2×10^{-8} Pa m^3 s^{-1}, GJB548A-96), as indicated in Table 2. The result showed the Al–diamond composites prepared by the LSS method had the advantages of high airtightness of chip integrated package and a wide spectrum of application prospect.

4 Conclusions

Al-based composites reinforced with 40 vol% diamond were fabricated by an advanced LSS process. The diamond powders were well dispersed in the composites that could be used for electronic packaging. Al_4C_3 phase could not been observed due to relatively low temperature sintering and separation. So far, the fabricated Al–diamond composites could have around 2 % porosity that was related to the conditions of diamond surface. The quality of the composite fabricated by LSS process is still on the way to be improved.

The TC of the composites reinforced with Ni-coated diamond reached 174 W m^{-1} K^{-1}, which increased about 11.7 %, compared with the composites reinforced without coated diamond. The obtained experimental values were approximately 79 % that of the calculation using Maxwell theoretical model.

The CTE values of the composites reinforced by coated or without coated Ni diamonds were similar, which were almost the same or just a little bit lower than the values obtained by Kerner simulation.

Based on the experimental results from Al composites reinforced by Ni-coated diamonds, the interface bonding between aluminum matrix and diamond reinforcement was the key to improve the material quality and TC value. An appropriate surface modification of diamond powders, combined with LSS process will be good to manufacture high quality composites in the application of heat dissipation.

Acknowledgments This work was financially supported by the Science Research Program of Beijing Municipal Commission of Education (00012125), (00012228).

References

1. Z.Y. Cai, R.C. Wang, C. Zhang, C.Q. Peng, L.Q. Wang, J. Mater. Sci. Mater. Electron. **26**, 4234 (2015)
2. M. Schöbel, H.P. Degischer, S. Vaucher, M. Hofmann, P. Cloetens, Acta Mater. **58**, 6421 (2010)
3. Q.P. Wang, F.F. Min, J.B. Zhu, J. Mater. Sci. Mater. Electron. **24**, 1937 (2012)
4. F.A. Khalid, O. Beffort, U.E. Klotz, B.A. Keller, P. Gasser, Diam. Relat. Mater. **13**, 393 (2004)
5. W. Yang, K. Peng, L. Zhou, J. Zhu, D. Li, Comput. Mater. Sci. **83**, 375 (2014)
6. P.W. Ruch, O. Beffort, S. Kleiner, L. Weber, P.J. Uggowitzer, Compos. Sci. Technol. **66**, 2677 (2006)
7. M. Caccia, A. Rodríguez, J. Narciso, JOM **66**, 920 (2014)
8. K.C. Collins, S. Chen, G. Chen, Appl. Phys. Lett. **97**, 083102 (2010)
9. H. Kwon, M. Leparoux, J.M. Heintz, J.F. Silvain, A. Kawasaki, Met. Mater. Int. **17**, 755 (2011)
10. M. Battabyal, O. Beffort, S. Kleiner, S. Vaucher, L. Rohr, Diam. Relat. Mater. **17**, 1438 (2008)
11. J. Shi, R.C. Che, C.Y. Liang, Y. Cui, S.B. Xu, L. Zhang, Compos. Part B Eng. **42**, 1346 (2011)
12. J.H. Wu, H.L. Zhang, Y. Zhang, J.W. Li, X.T. Wang, Mater. Des. **39**, 87 (2012)
13. X. Liang, C. Jia, K. Chu, H. Chen, J. Nie, W. Gao, J. Compos. Mater. **46**, 1127 (2012)
14. Z. Tan, Z. Li, G. Fan, X. Kai, G. Ji, L. Zhang, D. Zhang, Compos. Part B Eng. **47**, 173 (2013)
15. I.E. Monje, E. Louis, J.M. Molina, Compos. Part A Appl. Sci. Manuf. **67**, 70 (2014)
16. Q. Zhang, L.T. Jiang, G.H. Wu, J. Mater. Sci. Mater. Electron. **25**, 604 (2014)
17. C. Monachon, L. Weber, Diam. Relat. Mater. **39**, 8 (2013)
18. Y. Yamamoto, T. Imai, K. Tanabe, T. Tsuno, Y. Kumazawa, N. Fujimori, Diam. Relat. Mater. **6**, 1057 (1997)
19. Z.Q. Tan, Z.Q. Li, D.B. Xiong, G.L. Fan, G. Ji, D. Zhang, Mater. Des. **55**, 257 (2014)
20. Y.X. Li, J.Y. Liu, W.S. Wang, G.Q. Liu, Trans. Nonferr. Met. Soc. China **23**, 970 (2013)
21. Q.J. Jia, J.Y. Liu, Y.X. Li, W.S. Wang, Trans. Nonferr. Met. Soc. China **23**, 80 (2013)
22. O. Beffort, F.A. Khalid, L. Weber, P. Ruch, U.E. Klotz, S. Meier, S. Kleiner, Diam. Relat. Mater. **15**, 1250 (2006)
23. P.M. Geffroy, T. Chartier, J.F. Silvain, J. Eur. Ceram. Soc. **27**, 291 (2007)
24. R.J. Stoner, H.J. Maris, Phys. Rev. B Condens. Matter **48**, 16373 (1994)
25. A.M. Abyzov, F.M. Shakhov, A.I. Averkin, V.I. Nikolaev, Mater. Des. **87**, 527 (2015)
26. J.C. Maxwell, *An Elementary Treatise on Electricity*, 2nd edn. (Dover Publications, New York, 2011)
27. J.M. Molina, M. Rhême, J. Carron, L. Weber, Scr. Mater. **58**, 393 (2008)
28. R. Tavangar, J.M. Molina, L. Weber, Scr. Mater. **56**, 357 (2007)
29. M. Kida, L. Weber, C. Monachon, A. Mortensen, J. Appl. Phys. **109**, 064907 (2011)
30. D.P.H. Hasselman, J. Compos. Mater. **21**, 6869 (1987)
31. T.H. Nam, G. Requena, P. Degischer, Compos. Part A Appl. Sci. Manuf. **39**, 856 (2008)
32. B.K. Jang, J. Alloys Compd. **480**, 806 (2009)
33. E.H. Kerner, Proc. Phys. Soc. **69**, 808 (2002)